

Neuronal Excitability

# Functional Dissection of Ipsilateral and Contralateral Neural Activity Propagation Using Voltage-Sensitive Dye Imaging in Mouse Prefrontal Cortex

Pooja Gusain,<sup>1</sup> Makiko Taketoshi,<sup>1</sup> Yoko Tominaga,<sup>1</sup> and  Takashi Tominaga<sup>1,2</sup><https://doi.org/10.1523/ENEURO.0161-23.2023><sup>1</sup>Institute of Neuroscience, Tokushima Bunri University, Sanuki 769-2193, Japan and <sup>2</sup>Kagawa School of Pharmaceutical Sciences, Tokushima Bunri University, Sanuki 769-2193, Japan

## Abstract

Prefrontal cortex (PFC) intrahemispheric activity and the interhemispheric connection have a significant impact on neuropsychiatric disorder pathology. This study aimed to generate a functional map of FC intrahemispheric and interhemispheric connections. Functional dissection of mouse PFCs was performed using the voltage-sensitive dye (VSD) imaging method with high speed (1 ms/frame), high resolution (256 × 256 pixels), and a large field of view (~10 mm). Acute serial 350 μm slices were prepared from the bregma covering the PFC and numbered 1–5 based on their distance from the bregma (i.e., 1.70, 1.34, 0.98, 0.62, and 0.26 mm) with reference to the Mouse Brain Atlas (Paxinos and Franklin, 2008). The neural response to electrical stimulation was measured at nine sites and then averaged, and a functional map of the propagation patterns was created. Intracortical propagation was observed in slices 3–5, encompassing the anterior cingulate cortex (ACC) and corpus callosum (CC). The activity reached area 33 of the ACC. Direct white matter stimulation activated area 33 in both hemispheres. Similar findings were obtained via Dil staining of the CC. Imaging analysis revealed directional biases in neural signals traveling within the ACC, whereby the signal transmission speed and probability varied based on the signal direction. Specifically, the spread of neural signals from cg2 to cg1 was stronger than that from cingulate cortex area 1 (cg1) to cingulate cortex area 2 (cg2), which has implications for interhemispheric functional connections. These findings highlight the importance of understanding the PFC functional anatomy in evaluating neuromodulators like serotonin and dopamine, as well as other factors related to neuropsychiatric diseases.

**Key words:** anterior cingulate cortex; corpus callosum; medial prefrontal cortex; voltage-sensitive dye

## Significance Statement

This study used wide-field, high-speed, and high-resolution VSD imaging (VSDI) to create a real-time functional map of intrahemispheric and interhemispheric connections in the PFC of mice. The PFC and ACC have critical roles in neuropsychiatric disorders, and the study found that neural signals within the ACC exhibit directional biases, which could affect interhemispheric functional connections. This finding could pave the way for more effective neuropsychiatric disorder treatments. The functional map created with VSDI is a potent tool for exploring functional connections in the brain and could provide valuable insights into how the brain processes information.

Received May 15, 2023; accepted November 10, 2023; First published November 17, 2023.

The authors declare no competing financial interests.

Author contributions: P.G., Y.T., and T.T. designed research; P.G., M.T., Y.T., and T.T. performed research; P.G., Y.T., and T.T. contributed unpublished reagents/analytic tools; Y.T. and T.T. analyzed data; and P.G. and T.T. wrote the paper.

## Introduction

The prefrontal cortex (PFC; Laubach et al., 2018) is central to the integration of higher brain activities, such as working memory (Goldman-Rakic, 1995), mnemonic memory (Johnson et al., 2021), and social cognition (Apps et al., 2016). Accordingly, its disruption can cause schizophrenic and other neuropsychiatric phenotypes (Ghosal et al., 2017; Yan and Rein, 2022). In particular, the interhemispheric connection within the PFC through the corpus callosum (CC) plays a vital role in the pathology of these abnormalities (Aboitiz and Montiel, 2003; Tovar-Moll et al., 2007; Walker et al., 2012; Fenlon and Richards, 2015; Rovira and Geijo-Barrientos, 2016; Fenlon et al., 2021; Kilroy et al., 2022). The CC, particularly the anterior CC, participates in interhemispheric bilateral propagation of epileptic discharges (Musgrave and Gloor, 1980; Brodovskaya et al., 2022), and is, thus, a focus for the surgical treatment of epilepsy (Asadi-Pooya et al., 2008; Bullinger et al., 2022). However, the mechanism by which ipsilateral neural activity propagates to the CC and spreads to the contralateral hemisphere, especially in the frontal lobe, is not well understood.

Voltage-sensitive dye (VSD) imaging (VSDI) can directly visualize primary neuronal signals, including excitatory and inhibitory signals. Most functional imaging methods measure slow metabolic activity and secondary messenger ( $\text{Ca}^{2+}$ ) levels. However, real-time imaging techniques with high speed and high resolution have become necessary as interactions within and between cortical columns/hemispheres occur on a millisecond timescale. Therefore, tracking neuronal computations at the fundamental level of cortical columns in real time requires a spatial resolution of  $\sim 100\ \mu\text{m}$  and a temporal resolution of  $\sim 1\ \text{ms}$  (Buzsáki et al., 2012; Knöpfel and Song, 2019; Newton et al., 2021). Optical recording methods involving the external application of a dye (i.e., VSD) and high-speed and high-resolution capabilities will be advantageous in visualizing the broad correlations among brain areas from different angles *ex vivo* (Tanifuji et al., 1994; Iijima et al., 1996; de Curtis et al., 1999; Jin et al., 2002; Yuste, 2008). VSDI has shown high effectiveness in depicting various interactions among regions of the brain circuit and has been established as a quantitative and useful measurement tool (Tominaga et al., 2000, 2018, 2019) covering a wide area (Kajiwara et al., 2019; Kajiwara and Tominaga, 2021). Understanding how neural interactions are organized across multiple levels in the brain may provide a basis for fully elucidating higher brain functions in the PFC.

The main objective of this study was to create a functional map of the intrahemispheric and interhemispheric

connections of the PFC in mice. To achieve this goal, we used the VSDI technique, which has been widely adopted in neuroscience research (Salzberg et al., 1973; Cohen et al., 1978; Cohen and Salzberg, 1978; Homma et al., 2009; Peterka et al., 2011; Tominaga et al., 2013; Roome and Kuhn, 2020), to visualize brain activity. Specifically, we used a specially designed wide-field imaging system equipped with high-speed, high-resolution capabilities and a large imager. With this system, we were able to record neural activity across the entire coronal slice of the PFC. The application of this system facilitated the construction of a detailed functional map of intrahemispheric and interhemispheric connections of the PFC, which is critical for understanding the neural mechanisms underlying neuropsychiatric disorders.

## Materials and Methods

### Animals

C57BL/6N male mice aged 4–8 weeks were obtained from a distributor (Japan SLC). All animal experiments were approved by the Animal Care and Use Committee of Tokushima Bunri University (#KP21-83–2, #KP22-83–2). All applicable international, national, and/or institutional guidelines for the care and use of animals were followed.

### Preparing brain slices and VSD staining

Mice were anesthetized with isoflurane in a fume hood. The brain was then immediately resected and placed in cold artificial CSF (ACSF) solution containing the following (in mM): 124 NaCl, 2.5 KCl, 2  $\text{CaCl}_2$ , 2  $\text{MgSO}_4$ , 1.25  $\text{NaH}_2\text{PO}_4$ , 26  $\text{NaHCO}_3$  and 10 glucose, pH 7.4, for 5 min. Thereafter, the PFC was sectioned into 350- $\mu\text{m}$ -thick coronal slices using a vibrating slicer (VT-1000 or VT-1200; Leica Microsystems; Fig. 1A). Each slice was transferred into a special holder with a membrane filter (Tominaga et al., 2000, 2019) designed to keep the slices viable and maintain their order. The sections were then compared with the images on an atlas (Paxinos and Franklin, 2008) and labeled slice (SL)1–SL5 according to their distance from the bregma, 1.70, 1.34, 0.98, 0.62, and 0.26 mm (Fig. 1A).

Five slices were collected from each animal ( $n = 8$ ). All sections were then transferred to a humid chamber containing ACSF solution and a continuous supply of 95%  $\text{O}_2$ /5%  $\text{CO}_2$  mixed gas. The slices were incubated at 28°C for 25 min and stored at room temperature (22–26°C) for  $\sim 10$ –15 min before VSD staining. After 40 min of incubation, each slice was stained with 110  $\mu\text{l}$  of VSD solution for 20 min. The dye solution contained 0.2 mM Di-4-ANEPPS in 2.5% ethanol, 0.13% Cremophor EL, 1.17% distilled water, 48.1% fetal bovine serum, and 48.1% ACSF (Tominaga et al., 2000, 2013, 2019, 2023).

### Optical recording

Each slice was placed in the recording chamber with a continuous perfusion of oxygenated ACSF (bubbled with a 95%/5%  $\text{O}_2$ / $\text{CO}_2$  gas mixture) at a rate of 1 ml/min. To maintain cortical activity similar to that observed *in vivo*, all the data presented in this article were collected under perfusion of 1  $\mu\text{M}$  SR95531 (gabazine; Tocris Bioscience).

This work was supported by Japan Society for the Promotion of Science Grants JP23K18485, JP22H05698, JP21H03606, JP21K06702, JP21H03532, JP21H00447, JP20H04341, JP19H01142, JP16H06532 to T.T., and JP21K15247 to Y.T.

Correspondence should be addressed to Takashi Tominaga at tominagat@kph.bunri-u.ac.jp.

<https://doi.org/10.1523/ENEURO.0161-23.2023>

Copyright © 2023 Gusain et al.

This is an open-access article distributed under the terms of the Creative Commons Attribution 4.0 International license, which permits unrestricted use, distribution and reproduction in any medium provided that the original work is properly attributed.

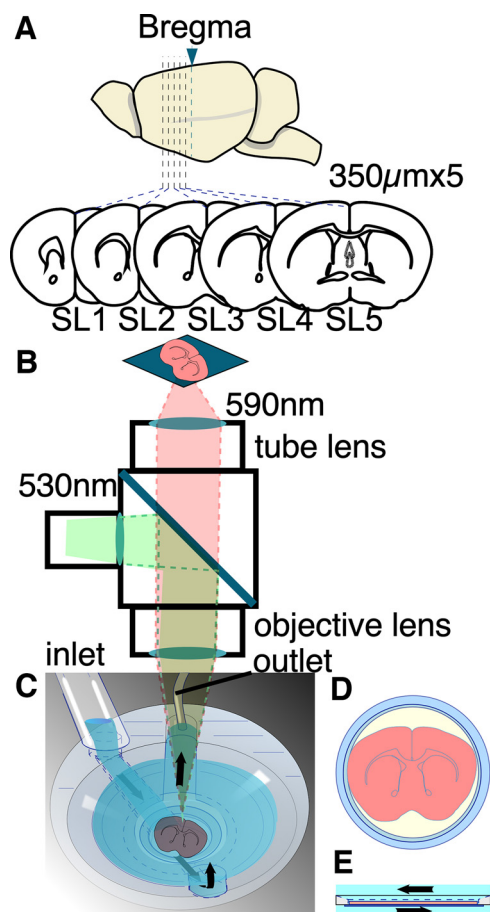


**Figure 1.** Schematics of slice preparation and experimental apparatus. **A**, Schematic illustration of mouse brain slices. The slices (350  $\mu\text{m}$  thickness) are continuously made from mouse brain. Each slice (5 slices per animal) is classified into SL1–SL5 depending on its morphology with reference to the brain atlas. SL1 refers to the slice collected 17.0 mm away from the bregma; SL2, 1.34 mm; SL3, 0.98 mm; SL4, 0.62 mm; and SL5, 0.26 mm. **B**, Schematic illustration of the optical recording system. To briefly summarize the experimental setup, the excitation light first passed through a bandpass filter (530  $\pm$  30 nm) and was then reflected by a dichroic mirror and directed toward the specimen. The resulting fluorescence was captured using a long-pass filter ( $>$ 590 nm) and projected onto an imager. The optical system consisted of an objective lens and a tube lens with the same  $F$  value, resulting in a total magnification of one. **C–E**, Recording chamber used for stabilizing the slice on a membrane filter (**D**) and for passing gas and fluid beneath the filter (**E**). The ACSF was delivered through the inlet and perfused from the bottom of the slice before being removed via the outlet.

This approach has been previously used to suppress excessive inhibitory synaptic transmission that can occur because of differences in the slice condition compared with *in vivo* conditions, thereby preserving cortical activity (Iijima et al., 1996; Kajiwara et al., 2019). Epifluorescence optics with two identical lenses ( $\times 1$  objective lens for a stereo microscope MZ series; catalog #10450028, Leica Microsystems) were used to visualize the slices—one for an objective and the other as a tube lens (Fig. 1B). The stained sections were illuminated with an excitation light

from a stabilized LED light source (LEX2-LZ4; Brain Vision) passed through a filter (530  $\pm$  30 nm). The amount of fluorescence generated by the stained section was passed through an emission filter ( $>$ 590 nm) and projected onto a camera.

To capture a wide range of neural activity, we used a specially designed wide-field imaging system with high-speed, high-resolution capabilities and a large imager (MiCAM05, Brain Vision). This system allowed us to record neural activity in the entire coronal slice at a high frame rate (1 ms/frame unless otherwise stated) and a high spatial resolution (256  $\times$  256 pixels). A microcapillary glass (outer diameter, 1.0 mm; inner diameter, 0.75 mm) filled with ACSF solution was used as the stimulating electrode. A ground electrode filled with 3 M KCl solution was used to avoid potential differences during the experiment. After the stimulation electrode was placed on the slice, the recording began. The stimulation frequency was set every 20 s for four sets for each slice. The data obtained were then analyzed using the BV analysis program (Brain Vision Analyzer, Brain Vision) and a custom application program on Igor Pro (versions 8 and 9, WaveMetrics). For numerical and statistical evaluations, a specially designed macro within Igor Pro software was used. The study incorporated the multiple-comparison Tukey's (HSD) test function within Igor Pro for all statistical analyses. Vector field analysis, which investigated neural activity propagation recorded via the VSD signal, was executed using the gradient function in the Python (version 3.9.16) Numpy package (version 1.23.5).

Electrical stimulation was provided with a glass electrode filled with ACSF ( $<$ 1 M $\Omega$ , bipolar 40 V, 0.5 ms each) to nine different sites in the slice [motor cortex, anterior cingulate cortex (ACC), and CC; Fig. 1D] from a stimulator (ESTM-8, Brain Vision).

### Neuronal tracing

To label the callosal neurons, solid DiI18(3) crystals (catalog #041-33423, FUJIFILM Wako Chemicals) were added to the ACC sections under microscope guidance. Briefly, DiI crystals were added to the cingulate cortex in the ipsilateral hemisphere using a glass micropipette with a sharp, elongated tip. To ensure delivery of the dye to the surface, the slices were gently poked with the pipette containing the DiI crystal. Given the slower diffusion of the dye in the cortex, the slices were maintained in an oxygenated medium (bubbled with a 95%/5% O<sub>2</sub>/CO<sub>2</sub> gas mixture) for 5–6 h. Finally, the slices were fixed with 4% paraformaldehyde and incubated at room temperature for 1–2 d to further ensure complete diffusion of the dye. Slices with 4% fixative were first bathed in 10 $\times$  PBS for 30 min and then analyzed.

### Laser confocal microscopic imaging

The stained sections were imaged using an LSM 510 META microscope (Zeiss). All images were captured using ACHROPLAN 40 $\times$ /0.80 w with a frame size of 1024  $\times$  1024. The fluorescence emitted by DiI 543 nm was visualized using a helium/neon laser with the following configurations: HFT 480/543 main beam splitter, NFT 545 (secondary

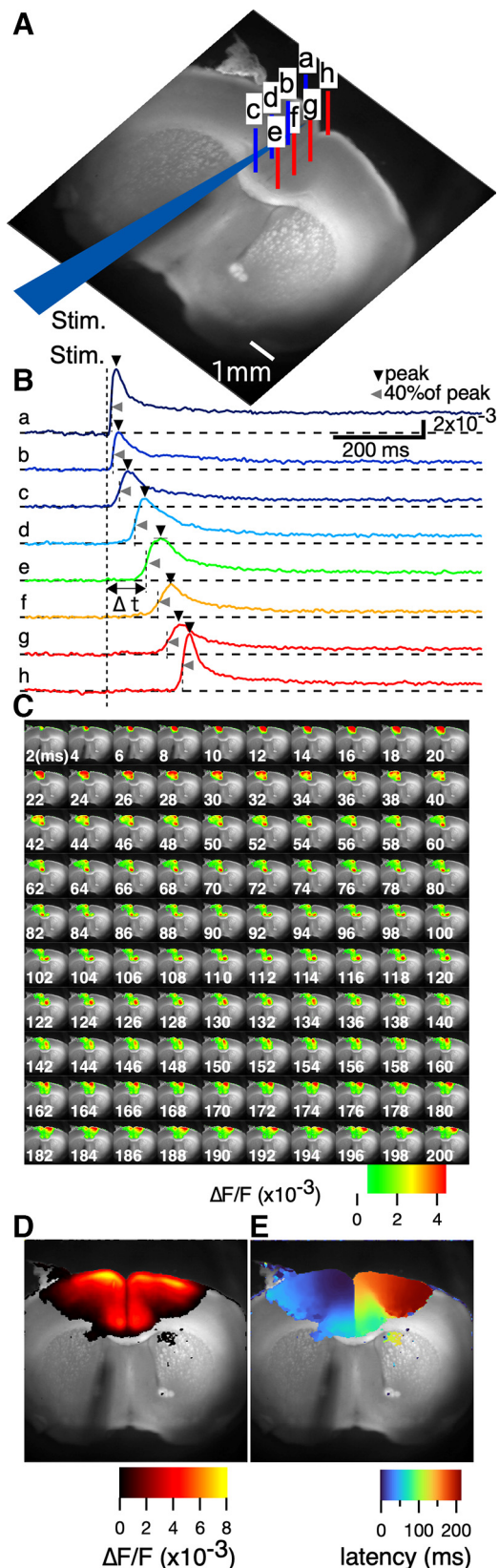


**Figure 2.** Contralateral spread of activity after electrical stimulation to the ACC. **Aa–h**, Configuration of SL 3 (obtained 0.98 mm from the bregma) and the stimulation electrode. **Ba–h**, Traces showing the optical signals at each pixel shown in **Aa–h**. The

continued

vertical dotted line shows the timing of the stimulation (Stim.; 40 V, 300  $\mu$ s bipolar). **C**, Pseudocolored consecutive images of the optical signal at each time section (frame rate, 1 ms/frame). The numbers in the images indicate the time (ms) after the stimulation. **D**, Color-coded projection of the peak values of each optical signal at each pixel in the field of view. **E**, Color-coded projection map of the latency ( $\Delta t$  in **B**; time to 40% of peak) to the initial response from stimulation time at each pixel in the field of view.

dichroic beam splitter), and LP505 BP 565–615 (bandpass filter).

## Results

### Intrahemispheric and interhemispheric propagations

Electrical stimulation of the superficial layer (layer II/III) of the ACC [cingulate cortex area 1 (cg1)] in SL3 (0.98 mm from the bregma; Fig. 2A) elicited a transient depolarizing optical response at the site of stimulation (Fig. 2Ba). The optical signal at the pixel propagated to the medial side of the stimulated (ipsilateral) cortex (Fig. 2Ba–d, blue traces). The propagation then spread across the interhemispheric connection to the contralateral cortex (i.e., other side of the cortex; Fig. 2Be–h, red). Figure 2C shows the propagation as the amplitude of the optical signal at each time slice (1 ms/frame) in pseudocolor in the ipsilateral and contralateral cortex. The septal-directed propagation along the ACC reached the distal end of cingulate cortex area 2 (cg2) within 39 ms (Fig. 2C). It then propagated to the contralateral side. The response appeared in the lower part of cg2 on the contralateral side within  $\sim 49$  ms. The wavefront of activity then moved to the dorsal side of the slice along with the ACC.

The propagation occurred as the wavefront of the activity appeared perpendicular to the layer structure of the cortex, indicating that the entire layer demonstrated consistent latency. For further analysis of functional activity mapping, we summarized the dynamic data in both the amplitude and time domains. The projection of the maximum peak,  $V_{\text{peak}}$  as visualized in Figure 2Ba, surpasses a threshold value of  $0.5 \times 10^{-3}$  and is displayed in Figure 2D in pseudocolor. The pattern of the activation amplitude map showed symmetry relative to the midline. The time that elapsed from the point of stimulation, marked by the dashed line to  $t_0$  in Figure 2B, was determined when the signal amplitude achieved 40% of its peak, denoted as  $\Delta t$  in Figure 2Bh. This latency for each pixel is color represented in the latency map shown in Figure 2E, adhering to the same threshold applied in Figure 2D. The activity propagated from the stimulation site and crossed the hemispheric boundary. The amplitude map delineates the neuronal networks activated within the cortical tissue, whereas the latency map reveals the order of their activation.

### Neuronal activation on different stimulation

To determine whether the same neural circuit is consistently activated by stimulation applied to different sites, we characterized which area is activated (amplitude maps) and how these circuits respond (latency maps) in the

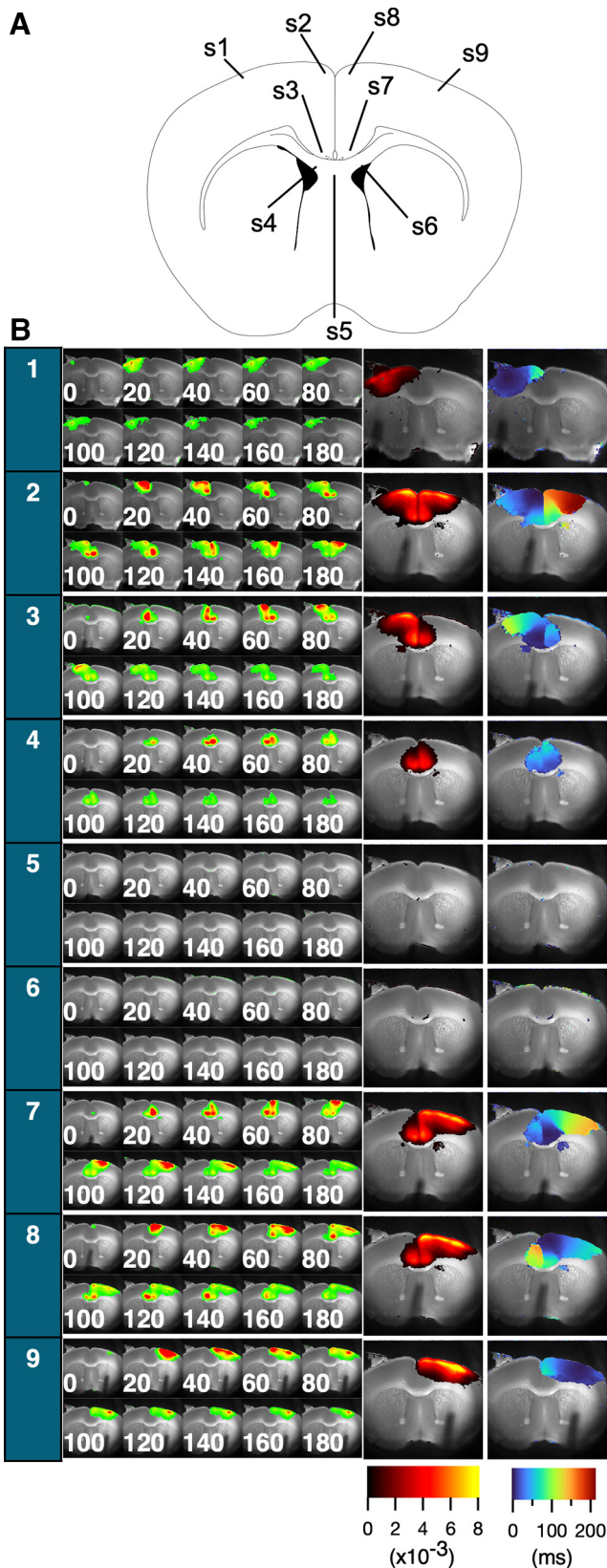


**Figure 3.** The figure displays consecutive images of the optical response (A), as well as projections of peak values and latencies for each stimulation site (B). Far left, Column corresponding to the site numbers (see above, Materials and Methods). The optical

*continued*

signal following stimulation is represented by 10 consecutive images, with each image numbered with a time point separated by 20 ms intervals and presented as a pseudocolor. Right, The two images show the projection of the peak values and latencies from the time of stimulation, presented in pseudocolor code as amplitude and latency maps, respectively. The amplitude maps show the amount of  $\Delta F/F$  ( $\times 10^{-3}$ ), whereas the latency maps show the latency time in milliseconds, as indicated by the color bars (bottom right).

cortex. To this end, we stimulated nine different sites [stimulation site (s1-s9) in the slice [layer II/III of the motor cortex (s1, s9), cg1 and cg2 of ACC (s2, s8, s3, and s7), the site opposite cg2 (s4 and s6), and middle of CC (s5); Fig. 1D]. Figure 3A shows the activation pattern of each stimulation site (10 consecutive images every 20 ms from stimulation) and the projection map of amplitude and latency.

The amplitude maps revealed a similar pattern; however, in most cases (Fig. 3B, s1, s3, s4, s7, s8, and s9), the amplitude maps were within the broadest spread (Fig. 3B, s2). This suggested that the local activation of the neural circuit had a limited spreading capacity. Stimulation of both hemispheric cortices resulted in nearly identical activation patterns (s1 vs s9, s2 vs s8, and s3 vs s7). Activity in the ventral side of the ACC (cg2) was followed by activation of the lateral dorsal striatum. Stimulation of the white matter (S5 and S6) did not induce a clear response. Notably, white matter stimulations, although capable of inducing activation in adjacent cortical areas, generally necessitate a higher activation threshold than direct cortical stimulations. This might reflect inherent differences in the activation thresholds intrinsic to these respective regions.

**Mapping of the activity spread in different slices**

The amplitude and latency maps are essential for understanding the neuronal circuitry in the cortex as they provide information on the circuits recruited by local activation. By examining these maps, we can gain insights into the specific networks involved, which is critical for mapping and analyzing the complex neuronal circuits in the cortex. To create a functional map of the PFC, we constructed averaged images by selecting regions of interest that matched the morphology of different brain slices. This approach allowed us to identify patterns of neural activity across different areas of the PFC and generate a comprehensive functional map of this brain region. Figure 4A presents five amplitude maps obtained from a similar slice plane (SL3; 0.98 mm from the bregma) on the same surface stimulated at cg1 (S2). We created an averaged image from these five recordings (Fig. 4B, SL3/s2, highlighted in yellow) by cropping the region and applying affine convolution (rotation of the image). The averaged image on SL3/s2 represented data from five different animals. Figure 4B shows the averaged images over five different levels (SL1–SL5) in the nine stimulation sites (S1–S9). The far right images show the averaged fluorescence image from SL1 to SL5. The propagation pattern was similar between the left and right hemispheres. In the

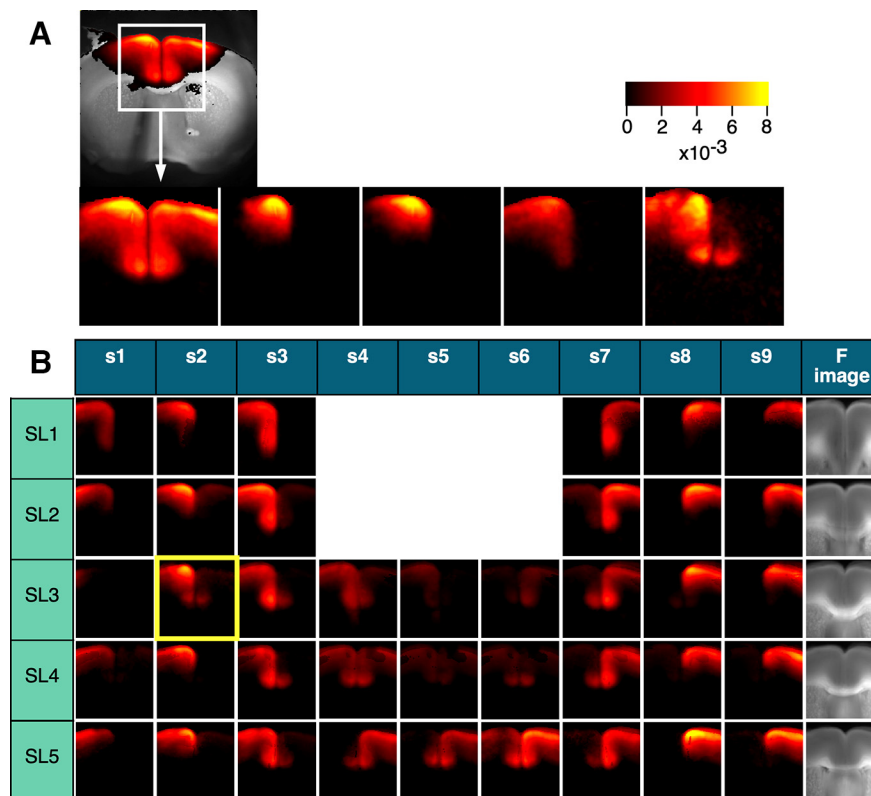


**Figure 4.** Map of the average peak-value projection across different slices. **A**, The variation of the same response to S2 in five different SL3 slices (0.98 mm from the bregma). **B**, Table of average peak-value projections in nine different stimuli (S1–S9) for five different slices (SL1–SL5). The averaged image highlighted in yellow (SL3/S2) is the average of five different responses shown in **A**. The averaged images are generated after affine conversion and trimming to best fit the shape of the slice;  $n = 6–8$  per image.

following section, we used all data from the same slice level to analyze the ipsilateral side (the stimulated side) on the left and the contralateral side on the right.

### Asymmetric propagation of the neuronal signal in the ACC

The propagation patterns within the ACC are shown in [Figure 5A](#) (amplitude). Dorsal surface stimulation caused limited propagation to the ventral side of the ACC, whereas ventral stimulation caused more extensive propagation to the dorsal side of the ACC. [Figure 5A](#) shows images of the ACC, with white lines indicating a vertical line overlaid on the images. In [Figure 5B](#), we present a plot of the amplitude profile along this vertical line, revealing how neural activity varies along this region of the ACC. The activity profiles induced by superficial stimulation rapidly decreased as the distance from the stimulation site increased. In contrast, deep stimulation produced a relatively flat amplitude profile along the line.

The propagation ratio is described in [Figure 5D](#), showing disparities in amplitude ratios at points most distant from the stimulation sites between dorsal (blue) and ventral (gray) stimulations. Notably, across all sectors (SL1–SL5), the propagation ratio manifested significantly more robustly during ventral stimulation than dorsal stimulation. This highlights an intrinsic asymmetric propagation mechanism within the ACC. Our observations indicate a

prevailing tendency for neural activity to propagate with enhanced intensity from the ventral to the dorsal regions of the medial PFC (mPFC). This inherent directional inclination in propagation mechanisms within the area appears to be intimately influenced by the prevailing pathways of information flow. Such observations furnish a nuanced understanding of the multifaceted roles of the mPFC in the processing and synthesis of information emanating from various brain regions. It further suggests the existence of specialized neuronal mechanisms within the mPFC, which are pivotal in facilitating these intricate processes.

### Cortical propagation velocity by area and direction

[Figure 6A](#) shows the average projection map of the pseudocolor rise time in SL3, calculated similarly to that in [Figure 5B](#). [Figure 6B](#) shows the line profiles of the latency along the cortex from the lateral side of the adjacent motor cortex to the medial ventral side toward the CC. The line profile for surface stimulation had minimum values of  $\sim 0.7$  mm (stimulation site) and increased in both directions. The line profile of deep stimulation had minimum values of  $\sim 2$  mm at the stimulation site, depending on the difference in the shape of the slices. The slope of the line profile tended to have a similar value but varied depending on the location and direction of propagation.

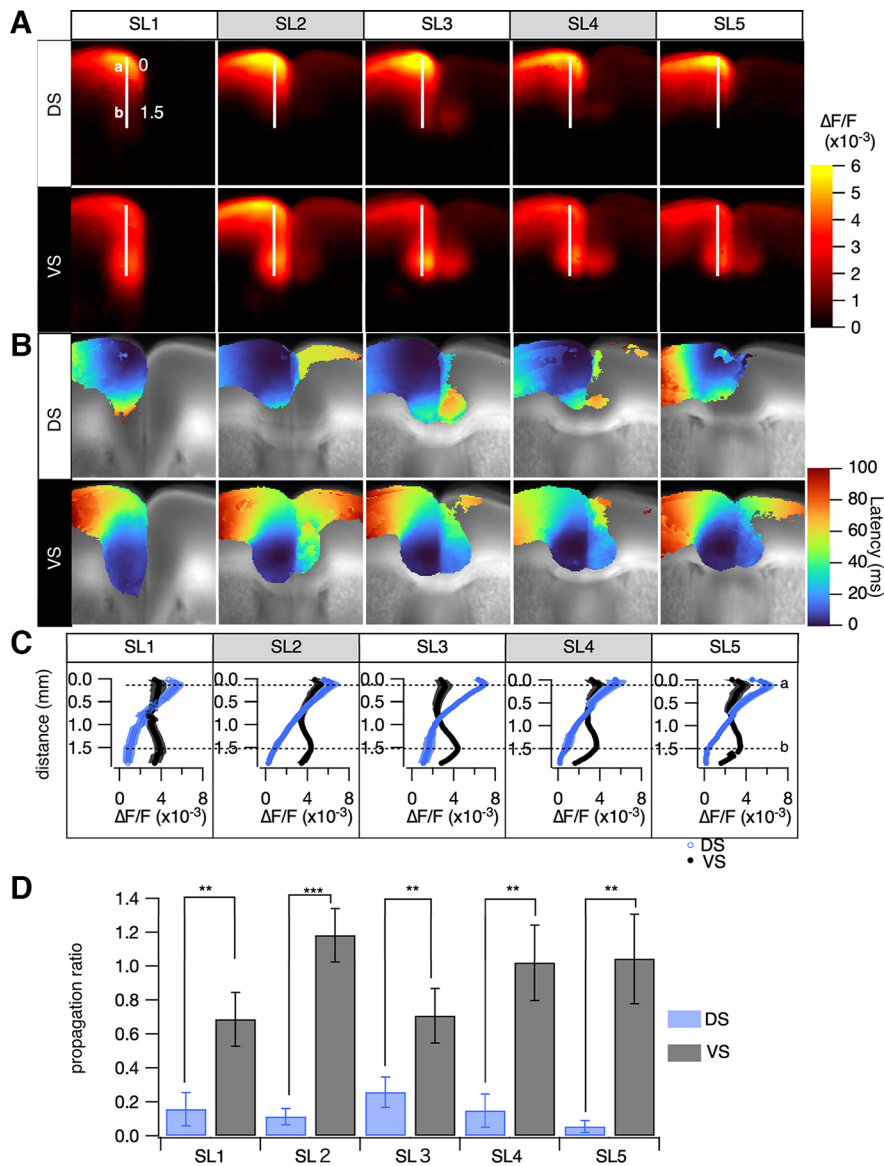


**Figure 5.** Analysis of uneven intrahemispheric neuronal propagation in the mPFC, comparing dorsal stimulation (DS) and ventral stimulation (VS) in layer II/III. **A**, The averaged peak projection image, arranged to position the stimulation site (ipsilateral hemisphere) on the left and the contralateral hemisphere on the right. **B**, The averaged latency projection, corresponding to **A**, with latency defined as the time to reach 40% of peak amplitude from stimulation onset at each pixel. **C**, Line profiles of peak projections (mean  $\pm$  SEM;  $n = 6-8$ ), depicting responses to DS (blue) and VS (black) along a specific line in **A**, ranging from SL1 to SL5. Right, Dashed lines (**a**, **b**) indicate locations nearest to the stimulation sites for DS and VS, respectively. **D**, The propagation ratio, derived from the intensity of the optical signals ( $\Delta F/F$ ) at the dashed lines in **C**. For DS, the ratio is ascertained by comparing the signal intensities at positions **a**, **b** (dorsal to ventral), whereas for VS, the calculation is inverted from **b** to **a** (ventral to dorsal). The bar graph elucidates these ratios (mean  $\pm$  SEM;  $n = 6-8$ ), facilitating a comparative evaluation of neuronal propagation variability between different stimulation sites; \*\* $p < 0.03$ , \*\*\* $p < 0.01$ .

The latency slope was an inverse function of the propagation velocity at that location. **Figure 6C** shows the propagation velocity measured at the cortical area (0–0.5 mm) and within the medial PFC (distance, 1.5–2.0 mm). The propagation speed in the medial PFC was almost always slower than that in the cortex, whereas it tended to be faster in the caudal slices when stimulation was applied ventrally. The speed of propagation in the cortex was consistently significantly higher under dorsal stimulation than

under stimulation in other areas. Meanwhile, when the propagation elicited in the deep dorsal side reached the cortex, the propagation tended to be slower, except for that between SL1 and SL3–SL5. The variation in propagation speed between cortical areas suggests that the mechanisms responsible for propagation differ based on cytoarchitecture. The target neural circuit for information transmission may differ depending on the stimulation direction (stimulation site).

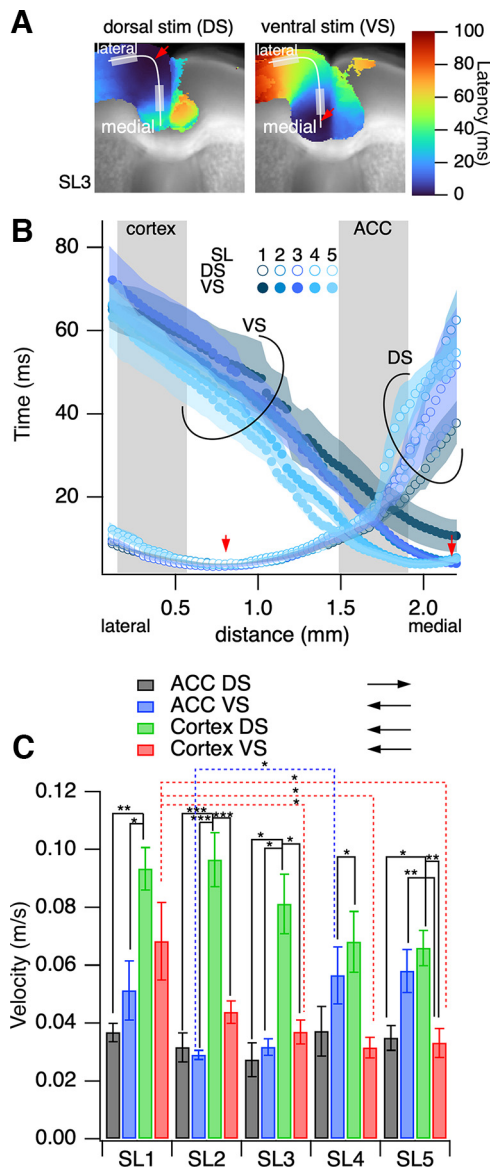


**Figure 6.** Analysis of intrahemispheric neuronal propagation in the mPFC on dorsal stimulation (DS) and ventral stimulation (VS) in layer II/III, to evaluate response latency. **A**, The averaged latency projection image is summarized as having the stimulation site (ipsilateral hemisphere) on the left-hand side and the other (contralateral hemisphere) on the right. **B**, The line profile of the latency along a line drawn on **A** (SL3) along layer II/III of the cortex on DS (open circle) and VS (solid circle). **C**, The propagation velocity is calculated as the inverse of the slope of the profile at the lateral cortex (LC) and the ACC on DS and VS. The plots show the mean  $\pm$  SEM,  $n = 8-12$ ;  $*p < 0.05$ ,  $**p < 0.03$ ,  $***p < 0.01$ .

**Interhemispheric propagation of neural signals in the medial cortex**

Interhemispheric propagation differed in the slices. Figure 7A summarizes the probability of occurrence of interhemispheric propagation according to ipsilateral activity that could cause contralateral activity at the dorsal end of the PFC. The probability of interhemispheric propagation was significantly higher in the slices near the bregma, where the medial

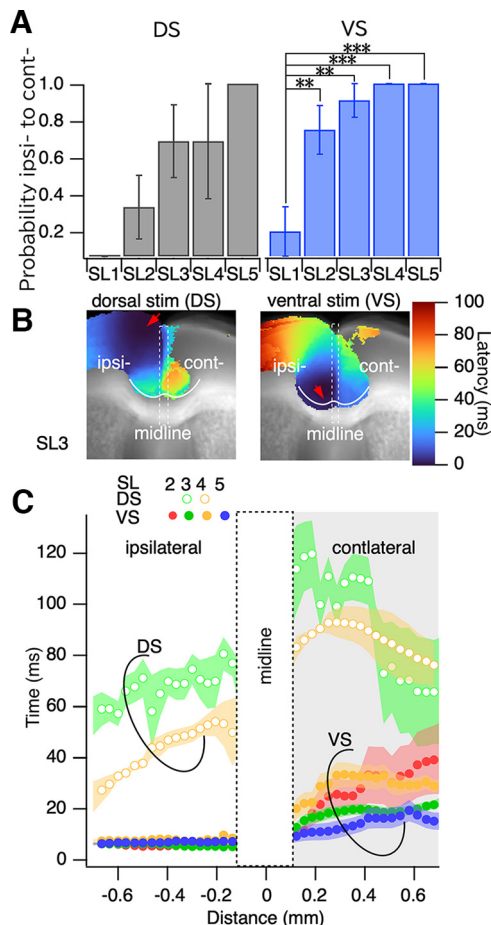


**Figure 7.** Interhemispheric connection. **A**, Probability of the occurrence of interhemispheric connection from the ipsilateral cortex to the contralateral cortex. **B**, Latency profile along the most ventral side of the medial prefrontal cortex drawn from the lateral end of the ipsilateral cortex to the contralateral cortex. **C**, Profile of the latency plot along the line for dorsal stimulation (DS; open circles) and ventral stimulation (VS; solid circles);  $n = 8-12$ ;  $**p < 0.03$ ,  $***p < 0.01$ .

cortex was the ACC, than in the slices farther from the bregma.

Deep stimulation in the ipsilateral side showed a small increase over time. The minimum latency value in the contralateral side was 20 ms (SL2–SL5), which was similar to that in the ipsilateral side, and then increased to 30 ms (SL2–SL5). Meanwhile, under surface stimulation, the latency was decreased in the outer border (deeper side) of the ACC and then increased toward the septal border, lasting 30 ms (SL3, SL4). The rise time values in the contralateral side were lowest in the deep layer of the ACC. This suggested that the deep layer of the ACC may be a site of CC connection between hemispheres, at least for coherent neural signal propagation.

**The site of interhemispheric propagation**

We addressed the site of interhemispheric connections in the ACC using high-speed focal imaging (300  $\mu$ s/frame; Fig. 8A). Neuronal activation from the left side of the slice



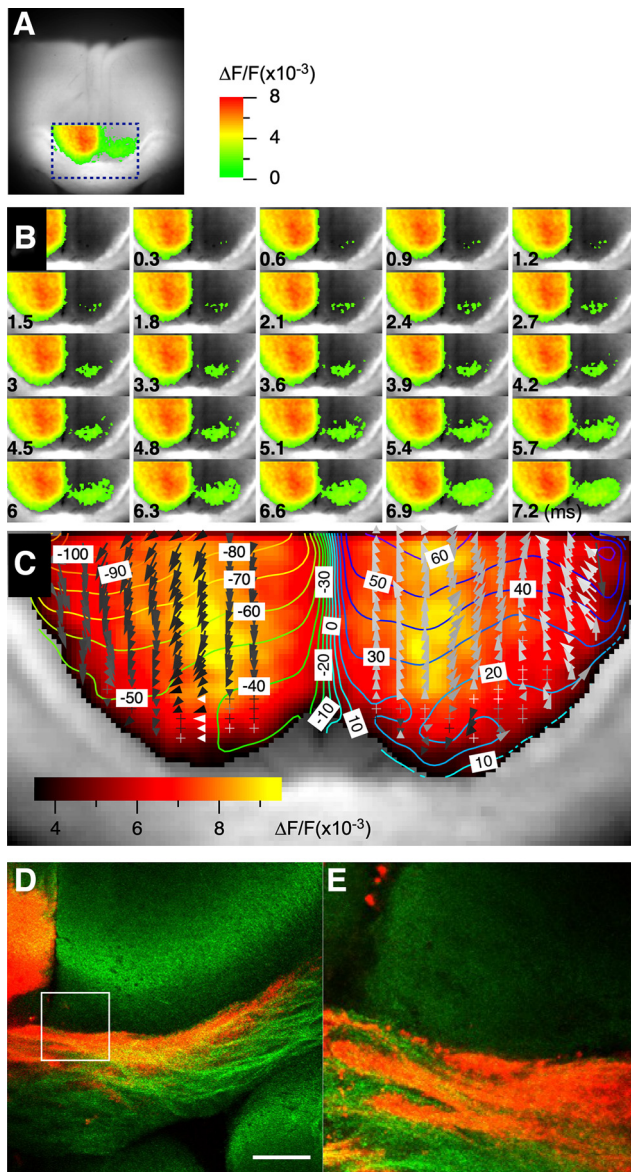


**Figure 8.** Site of interhemispheric propagation. **A**, Location of the focal high-speed imaging (300  $\mu\text{s}/\text{frame}$ ) used to study interhemispheric propagation in the ACC. **B**, Consecutive images taken at 300  $\mu\text{s}$  intervals during interhemispheric propagation of neuronal activity in the ACC. **C**, Amplitude map of the recorded activity superimposed with a contour plot and vector field representation of latency map, illustrating the direction and speed of the interhemispheric propagation. **D**, **E**, Representative images of Dil microdot staining in the ACC when the microdot was placed on the left side of the slice, showing the ipsilateral projection from the cingulate cortex and the corresponding interhemispheric callosal fiber projection to the contralateral side. Scale bar, 30  $\mu\text{m}$ .

propagated interhemispherically, with activity first appearing in the deep layer of cg2 (Fig. 8B). The interhemispheric propagation occurred on the outer rim of the ACC and spread toward the ventral side of the brain. To better visualize the propagation, we created a contour plot superimposed with a vector field graph indicating the propagation direction (Fig. 8C).

To examine the importance of the CC in the transmission of neuronal activity, we used a microsurgical technique with a fine microcapillary (outer diameter, 1.0 mm; inner diameter, 0.5 mm). Our findings showed that lesions made close to the center of the callosum terminated activity, blocking the connectivity between the ipsilateral and contralateral hemisphere of the ACC. This observation supports the speculation that the deep layer of cg2 serves as the connection site where the callosal fiber conveys the projection of neural activity from one side of the hemisphere to the other.

To further elucidate this perspective, we used the lipophilic neuronal tracer Dil crystal in our investigation. After applying the Dil crystal to the ipsilateral cingulate cortex, we observed that the labeled projections extended through the CC, terminating at the bottom of layer VI of cg2 on the contralateral side without further invasion into the contralateral structures (Fig. 8D,E). These findings highlight the pivotal role the deep layers of cg2 and callosal fiber projections play in determining the specific sites and functional connectivity associated with interhemispheric propagation in the ACC.

## Discussion

### Main findings

This study used VSDI to create a real-time functional map of intrahemispheric and interhemispheric connections in the PFC of mice. The ACC exhibited directional biases in neural signaling that could have an impact on interhemispheric functional connections. Specifically, differences in the propagation pattern among ACC areas were observed that affected interhemispheric propagation in the ACC. Moreover, we observed that the interhemispheric activity propagation within the ACC was particularly prominent in a specific region, cg2. This observation is remarkable given that the CC typically facilitates more widespread homotopic connections between the hemispheres (De León Reyes et al., 2020). These findings provide insights into the mechanisms responsible for neural signal propagation in the ACC and suggest potential targets for treating neuropsychiatric disorders. Furthermore, this study demonstrates the power of VSDI in investigating brain function and highlights the importance of exploring functional connections in the brain.

Here, a functional activity map of the PFC was generated using VSDI. Given that the anatomic definition of the rodent PFC is controversial (Laubach et al., 2018; van Heukelum et al., 2020), this study applied the nomenclature of Paxinos and Franklin (2008). Results revealed activity in the motor cortex (M1 and M2), ACC (cg1 and cg2), prelimbic and infralimbic cortex, and dorsal peduncular cortex. Additionally, evidence of activity was detected in parts of the dorsal lateral striatum (Fig. 2) and other cortical areas, particularly on the frontal side (mostly in SL1). These comprehensive data regarding the neural circuitry of the PFC were obtained because of the large field of view of the VSDI system, high spatial resolution (30  $\mu\text{m}$  per pixel), and high frame rate (1 ms/frame). These conditions are typically challenging to achieve as they can

easily lead to a reduced photon number at the imaging device, resulting in a poor signal-to-noise ratio.

In our study, we administered an electrical stimulation of  $\pm 40$  V, exerted biphasically for 500  $\mu$ s each. This level of stimulus strength was chosen based on its ability to elicit a maximal response in the CA1 area of mouse hippocampal slices, as supported by previous findings (Tominaga et al., 2019; Utsumi et al., 2023). Importantly, minor variations in the stimulation strength at this level had a negligible effect on the propagation pattern of activity within the cortical slices.

Within the mPFC and the interhemispheric region, the mode of propagation differed according to the propagation direction. Specifically, the neural signal propagating from the ventral to the dorsal cortical area (brain surface) had a greater probability of propagating from the CC to the dorsal cortical area. In contrast, activity from the cortex was strongly attenuated in the mPFC (Fig. 5). The mPFC has been implicated in several neuropsychiatric disorders. For instance, Strakowski et al. (2005, 2012) reported that emotional dysregulation in bipolar disorder results from the inability of the PFC to modulate anterior limbic structures such as the amygdala. Meanwhile, Ragland et al. (2007) concluded that the inefficiency in cognitive information processing in schizophrenia results from PFC dysfunction. Gilbert et al. (2006) also suggest that mPFC alterations contribute to impaired reality monitoring in schizophrenia (Gilbert et al., 2006). In addition, the ACC plays a pivotal role in pain-induced depression (Barthas et al., 2015), pain perception and chronic pain (Koga et al., 2015; Guo et al., 2022), and spinal sensory transmission (Chen et al., 2018). The present findings provide a functional map for investigating pathologic modifications in the PFC.

### Population propagation of neural activity under weak GABAergic blockade

The propagation of neural activity in layers II/III and intra-hemispheric connections under GABAergic blockade has been extensively studied using electrophysiological methods (Walker et al., 2012; Rovira and Geijo-Barrientos, 2016; Robles et al., 2020; Domínguez-Sala et al., 2022). However, the present study did not detect any oscillatory activity under these conditions, possibly because of the weak blockade of GABAergic systems. Nevertheless, the propagation of the initial inward discharge in the field potential recordings (Rovira and Geijo-Barrientos, 2016) was similar to that observed with VSD imaging; that is, the propagation speed of 30–40 mm/s was relatively the same as that observed under GABAergic blockade. VSDI allowed us to visualize the mechanisms by which the depolarizing signal propagated through the ACC and activated all layers almost simultaneously.

The coherent neural propagation observed in the PFC at 30–40 mm/s is common in other cortical areas, including the entorhinal, perirhinal, and visual cortices (Iijima et al., 1996; Yoshimura et al., 2016; Kajiwara et al., 2019; Kajiwara and Tominaga, 2021; Fukuda et al., 2023). Detailed modeling has previously shown that PFC networks with strong feedback inhibition exhibit resonance (Sherfey et al., 2018). Increasing experimental evidence also shows millisecond

fidelity and temporal reliability (Compte et al., 2000; Gollisch and Meister, 2008). With millisecond fidelity, precisely synchronized action potentials can propagate within a model of cortical network activity that mimics many of the characteristics of biological systems. This model demonstrates how time intervals and periodicity of operation can be determined by simulating synaptic learning in a neural circuit model based on neural connections (Durstewitz et al., 2000; He, 2019). Using a model of cortical network activity, Diesmann et al. (1999) showed that precisely synchronized action potentials can propagate with millisecond accuracy.

The cingulate cortex has been found to exhibit neural connectivity with motor areas on the lateral and medial surface of the brain as well as with the prefrontal cortex (Nauta, 1972; Vogt and Pandya, 1987; Koski and Paus, 2000). Neurons that facilitate interhemispheric connections project to the opposite cortex, particularly to the homotopic region of the brain (Tovar-Moll et al., 2007; Fame et al., 2011; Fenlon and Richards, 2015; De León Reyes et al., 2020; Szczupak et al., 2023).

The optical signal in this study did not show such direct activation of the homotopic region (Fig. 7). Rather, the optical signal propagated to the contralateral hemisphere at CG2 facing the CC. The results showed that microsurgery of the CC on the lateral side did not disrupt interhemispheric interaction, but resection in the middle of the CC disrupted propagation (Fig. 8). Although the initial stimulation was delivered to L2/3 cg1 and cg2, the neuronal activity captured by the VSD signal activated sequential propagation within the ACC and interhemispheric propagation to cg2. Although it is unclear whether this type of activity propagation carries physiological information, correlations of spikes from multiple neurons may have essential functions (Panzeri et al., 2022).

### Optical recording of cortical activity

Synchronized activity among cortical neurons is critical for normal brain function and allows the integration of information. Disruptions in this synchronized activity have been linked to various conditions, including epilepsy, schizophrenia, and Alzheimer's disease (Singer, 1993; McNamara, 1994; Pinto et al., 2005; Takahashi et al., 2015; Muller et al., 2018). Previous research has emphasized the importance of synchronous activity for working memory and cognitive deficits in schizophrenia (Takahashi et al., 2015; Muller et al., 2018). It is measured with various imaging techniques, including genetically encoded Ca indicators (Huang et al., 2010; Rynes et al., 2021) and genetically encoded voltage indicators (Knöpfel, 2012; Knöpfel and Song, 2019; Rhee et al., 2021). VSDI is also a reliable tool for visualizing these synchronizing activities in the cortex (Tanifuji et al., 1994; Iijima et al., 1996; de Curtis et al., 1999; Jin et al., 2002; Yuste, 2008; Fujieda et al., 2015; Yoshimura et al., 2016; Kajiwara et al., 2019; Kajiwara and Tominaga, 2021; Newton et al., 2021; Palkar et al., 2023). The large wide-field bright optics and the special chamber system (Tominaga et al., 2000, 2023), allowing stable fixation of the slices, enable characterization of large-scale cortical activity. The stable

long-term recording also enables the collection of a large volume of data (Tominaga et al., 2019).

One potential limitation of this study is that it used electrical stimulation to recruit neural activity, which can activate multiple elements of the neural circuitry. As such, it can be difficult to determine which specific neural pathways are activated and how this relates to the observed activity. This issue could be addressed using optogenetics, which allows for more precise control of neural activity by selectively activating specific populations of neurons with light (Yizhar et al., 2011). However, it should be noted that the combination of voltage imaging and optogenetics can add additional complexity to the study. For example, optogenetics can alter the characteristics of neural activity in ways that may not be fully understood or accounted for in the analysis.

Nevertheless, this study provides important insights into the mechanisms of neural propagation in the prefrontal cortex and the potential role of directional biases in interhemispheric communication. The findings of the study have implications in understanding the neural basis of neuropsychiatric disorders and could inform the development of more targeted interventions. Future studies could explore the use of optogenetics to overcome the limitations of electrical stimulation and to provide more precise control over neural activity in the prefrontal cortex and other brain regions.

## References

- Aboitiz F, Montiel J (2003) One hundred million years of interhemispheric communication: the history of the corpus callosum. *Braz J Med Biol Res* 36:409–420.
- Apps MAJ, Rushworth MFS, Chang SWC (2016) The anterior cingulate gyrus and social cognition: Tracking the motivation of others. *Neuron* 90:692–707.
- Asadi-Pooya AA, Sharan A, Nei M, Sperling MR (2008) Corpus callosotomy. *Epilepsy Behav* 13:271–278.
- Barthas F, Sellmeijer J, Hugel S, Waltisperger E, Barrot M, Yalcin I (2015) The anterior cingulate cortex is a critical hub for pain-induced depression. *Biol Psychiatry* 77:236–245.
- Brodovskaya A, Batabyal T, Shiono S, Sun H, Kapur J (2022) Distinct roles of rodent thalamus and corpus callosum in seizure generalization. *Ann Neurol* 91:682–696.
- Bullinger KL, Alwaki A, Gross RE (2022) Surgical treatment of drug-resistant generalized epilepsy. *Curr Neurol Neurosci Rep* 22:459–465.
- Buzsáki G, Anastassiou CA, Koch C (2012) The origin of extracellular fields and currents—EEG, ECoG, LFP and spikes. *Nat Rev Neurosci* 13:407–420.
- Chen T, Taniguchi W, Chen Q-Y, Tozaki-Saitoh H, Song Q, Liu R-H, Koga K, Matsuda T, Kaito-Sugimura Y, Wang J, Li Z-H, Lu Y-C, Inoue K, Tsuda M, Li Y-Q, Nakatsuka T, Zhuo M (2018) Top-down descending facilitation of spinal sensory excitatory transmission from the anterior cingulate cortex. *Nat Commun* 9:1886.
- Cohen LB, Salzberg BM (1978) Optical measurement of membrane potential. *Rev Physiol Biochem Pharmacol* 83:35–88.
- Cohen LB, Salzberg BM, Grinvald A (1978) Optical methods for monitoring neuron activity. *Annu Rev Neurosci* 1:171–182.
- Compte A, Brunel N, Goldman-Rakic PS, Wang X-J (2000) Synaptic mechanisms and network dynamics underlying spatial working memory in a cortical network model. *Cereb Cortex* 10:910–923.
- de Curtis M, Takashima I, Iijima T (1999) Optical recording of cortical activity after *in vitro* perfusion of cerebral arteries with a voltage-sensitive dye. *Brain Res* 837:314–319.
- De León Reyes NS, Bragg-Gonzalo L, Nieto M (2020) Development and plasticity of the corpus callosum. *Development* 147:dev189738.
- Diesmann M, Gewaltig M-O, Aertsen A (1999) Stable propagation of synchronous spiking in cortical neural networks. *Nature* 402:529–533.
- Domínguez-Sala E, Andreu-Cervera A, Martín-Climent P, Murcia-Ramón R, Martínez S, Geijo-Barrientos E (2022) Properties of the epileptiform activity in the cingulate cortex of a mouse model of LIS1 dysfunction. *Brain Struct Funct* 227:1599–1614.
- Durstewitz D, Seamans JK, Sejnowski TJ (2000) Dopamine-mediated stabilization of delay-period activity in a network model of prefrontal cortex. *J Neurophysiol* 83:1733–1750.
- Fame RM, MacDonald JL, Macklis JD (2011) Development, specification, and diversity of callosal projection neurons. *Trends Neurosci* 34:41–50.
- Fenlon LR, Richards LJ (2015) Contralateral targeting of the corpus callosum in normal and pathological brain function. *Trends Neurosci* 38:264–272.
- Fenlon LR, Suarez R, Lynton Z, Richards LJ (2021) The evolution, formation and connectivity of the anterior commissure. *Semin Cell Dev Biol* 118:50–59.
- Fujieda T, Koganezawa N, Ide Y, Shirao T, Sekino Y (2015) An inhibitory pathway controlling the gating mechanism of the mouse lateral amygdala revealed by voltage-sensitive dye imaging. *Neurosci Lett* 590:126–131.
- Fukuda T, Tominaga T, Tominaga Y, Kanayama H, Kato N, Yoshimura H (2023) Alternative strategy for driving voltage-oscillator in neocortex of rats. *Neurosci Res* 191:28–37.
- Ghosal S, Hare BD, Duman RS (2017) Prefrontal cortex GABAergic deficits and circuit dysfunction in the pathophysiology and treatment of chronic stress and depression. *Curr Opin Behav Sci* 14:1–8.
- Gilbert SJ, Spengler S, Simons JS, Frith CD, Burgess PW (2006) Differential functions of lateral and medial rostral prefrontal cortex (Area 10) revealed by brain-behavior associations. *Cereb Cortex* 16:1783–1789.
- Goldman-Rakic PS (1995) Cellular basis of working memory. *Neuron* 14:477–485.
- Gollisch T, Meister M (2008) Rapid neural coding in the retina with relative spike latencies. *Science* 319:1108–1111.
- Guo F, Du Y, Qu F-H, Lin S-D, Chen Z, Zhang S-H (2022) Dissecting the neural circuitry for pain modulation and chronic pain: insights from optogenetics. *Neurosci Bull* 38:440–452.
- He Z (2019) Cellular and network mechanisms for temporal signal propagation in a cortical network model. *Front Comput Neurosci* 13:57.
- Homma R, Baker BJ, Jin L, Garaschuk O, Konnerth A, Cohen LB, Bleau CX, Canepari M, Djuricic M, Zecevic D (2009) Wide-field and two-photon imaging of brain activity with voltage- and calcium-sensitive dyes. *Methods Mol Biol* 489:43–79.
- Huang X, Xu W, Liang J, Takagaki K, Gao X, Wu J (2010) Spiral wave dynamics in neocortex. *Neuron* 68:978–990.
- Iijima T, Witter MP, Ichikawa M, Tominaga T, Kajiwara R, Matsumoto G (1996) Entorhinal-hippocampal interactions revealed by real-time imaging. *Science* 272:1176–1179.
- Jin W, Zhang R-J, Wu J (2002) Voltage-sensitive dye imaging of population neuronal activity in cortical tissue. *J Neurosci Methods* 115:13–27.
- Johnson SA, Zequeira S, Turner SM, Maurer AP, Bizon JL, Burke SN (2021) Rodent mnemonic similarity task performance requires the prefrontal cortex. *Hippocampus* 31:701–716.
- Kajiwara R, Tominaga T (2021) Perirhinal cortex area 35 controls the functional link between the perirhinal and entorhinal-hippocampal circuitry. *Bioessays* 43:e2000084.
- Kajiwara R, Tominaga Y, Tominaga T (2019) Network plasticity involved in the spread of neural activity within the rhinal cortices as revealed by voltage-sensitive dye imaging in mouse brain slices. *Front Cell Neurosci* 13:20.
- Kilroy E, Gerbella M, Cao L, Molfese P, Butera C, Harrison L, Jayashankar A, Rizzolatti G, Aziz-Zadeh L (2022) Specific tractography differences in autism compared to developmental coordination disorder. *Sci Rep* 12:19246.

- Knöpfel T (2012) Genetically encoded optical indicators for the analysis of neuronal circuits. *Nat Rev Neurosci* 13:687–700.
- Knöpfel T, Song C (2019) Optical voltage imaging in neurons: moving from technology development to practical tool. *Nat Rev Neurosci* 20:719–727.
- Koga K, Descalzi G, Chen T, Ko H-G, Lu J, Li S, Son J, Kim TH, Kwak C, Haganir RL, Zhao M-G, Kaang B-K, Collingridge GL, Zhuo M (2015) Coexistence of two forms of LTP in ACC provides a synaptic mechanism for the interactions between anxiety and chronic pain. *Neuron* 85:377–389.
- Koski L, Paus T (2000) Functional connectivity of the anterior cingulate cortex within the human frontal lobe: a brain-mapping meta-analysis. In: *Executive control and the frontal lobe: current issues*. (Schneider WX, Owen AM, Duncan J, eds), pp 55–65. Berlin: Springer.
- Laubach M, Amarante LM, Swanson TK, White SR (2018) What, if anything, is rodent prefrontal cortex? *eNeuro* 5:ENEURO.0315-18.2018.
- McNamara J (1994) Cellular and molecular basis of epilepsy. *J Neurosci* 14:3413–3425.
- Muller L, Chavane F, Reynolds J, Sejnowski TJ (2018) Cortical traveling waves: mechanisms and computational principles. *Nat Rev Neurosci* 19:255–268.
- Musgrave J, Gloor P (1980) The role of the corpus callosum in bilateral interhemispheric synchrony of spike and wave discharge in febrile generalized penicillin epilepsy. *Epilepsia* 21:369–378.
- Nauta WJ (1972) Neural associations of the frontal cortex. *Acta Neurobiol Exp (Wars)* 32:125–140.
- Newton TH, Reimann MW, Abdellah M, Chevtchenko G, Muller EB, Markram H (2021) *In silico* voltage-sensitive dye imaging reveals the emergent dynamics of cortical populations. *Nat Commun* 12:3630.
- Palkar G, Wu J, Ermentrout B (2023) The inhibitory control of traveling waves in cortical networks. *PLoS Comput Biol* 19:e1010697.
- Panzeri S, Moroni M, Safaai H, Harvey CD (2022) The structures and functions of correlations in neural population codes. *Nat Rev Neurosci* 23:551–567.
- Paxinos G, Franklin KBJ (2008) *The mouse brain in stereotaxic coordinates*. New York: Elsevier.
- Peterka DS, Takahashi H, Yuste R (2011) Imaging voltage in neurons. *Neuron* 69:9–21.
- Pinto DJ, Patrick SL, Huang WC, Connors BW (2005) Initiation, propagation, and termination of epileptiform activity in rodent neocortex *in vitro* involve distinct mechanisms. *J Neurosci* 25:8131–8140.
- Ragland JD, Yoon J, Minzenberg MJ, Carter CS (2007) Neuroimaging of cognitive disability in schizophrenia: search for a pathophysiological mechanism. *Int Rev Psychiatry* 19:417–427.
- Rhee JK, Iwamoto Y, Baker BJ (2021) Visualizing oscillations in brain slices with genetically encoded voltage indicators. *Front Neuroanat* 15:741711.
- Robles RM, Domínguez-Sala E, Martínez S, Geijo-Barrientos E (2020) Layer 2/3 pyramidal neurons of the mouse granular retrosplenial cortex and their innervation by cortico-cortical axons. *Front Neural Circuits* 14:576504.
- Roome CJ, Kuhn B (2020) Voltage imaging with ANNINE dyes and two-photon microscopy of Purkinje dendrites in awake mice. *Neurosci Res* 152:15–24.
- Rovira V, Geijo-Barrientos E (2016) Intra- and interhemispheric propagation of electrophysiological synchronous activity and its modulation by serotonin in the cingulate cortex of juvenile mice. *PLoS One* 11:e0150092.
- Rynes ML, Surinach DA, Linn S, Laroque M, Rajendran V, Dominguez J, Hadjistamoulou O, Navabi ZS, Ghanbari L, Johnson GW, Nazari M, Mohajerani MH, Kodandaramaiah SB (2021) Miniaturized head-mounted microscope for whole-cortex mesoscale imaging in freely behaving mice. *Nat Methods* 18:417–425.
- Salzberg BM, Davila HV, Cohen LB (1973) Optical recording of impulses in individual neurones of an invertebrate central nervous system. *Nature* 246:508–509.
- Sherfey JS, Ardid S, Hass J, Hasselmo ME, Kopell NJ (2018) Flexible resonance in prefrontal networks with strong feedback inhibition. *PLoS Comput Biol* 14:e1006357.
- Singer W (1993) Synchronization of cortical activity and its putative role in information processing and learning. *Annu Rev Physiol* 55:349–374.
- Strakowski SM, DelBello MP, Adler CM, (2005) The functional neuroanatomy of bipolar disorder: a review of neuroimaging findings. *Mol Psychiatry* 10:105–116.
- Strakowski SM, Adler CM, Almeida J, Altshuler LL, Blumberg HP, Chang KD, DelBello MP, Frangou S, McIntosh A, Phillips ML, Sussman JE, Townsend JD (2012) The functional neuroanatomy of bipolar disorder: a consensus model. *Bipolar Disord* 14:313–325.
- Szczupak D, Lack PM, Rayée D, Liu C, Lent R, Tovar-Moll F, Silva AC (2023) The relevance of heterotopic callosal fibers to interhemispheric connectivity of the mammalian brain. *Cereb Cortex* 33:4752–4760.
- Takahashi N, Sawada W, Noguchi J, Watanabe S, Ucar H, Hayashi-Takagi A, Yagishita S, Ohno M, Tokumaru H, Kasai H (2015) Two-photon fluorescence lifetime imaging of primed SNARE complexes in presynaptic terminals and  $\beta$  cells. *Nat Commun* 6:8531.
- Tanifuji M, Sugiyama T, Murase K (1994) Horizontal propagation of excitation in rat visual cortical slices revealed by optical imaging. *Science* 266:1057–1059.
- Tominaga T, Tominaga Y, Yamada H, Matsumoto G, Ichikawa M (2000) Quantification of optical signals with electrophysiological signals in neural activities of Di-4-ANEPPS stained rat hippocampal slices. *J Neurosci Methods* 102:11–23.
- Tominaga T, Kajiwara R, Tominaga Y (2013) VSD imaging method of *ex vivo* brain preparation. *J Neurosci Neuroengng* 2:211–219.
- Tominaga Y, Taketoshi M, Tominaga T (2018) Overall assay of neuronal signal propagation pattern with long-term potentiation (LTP) in hippocampal slices from the CA1 area with fast voltage-sensitive dye imaging. *Front Cell Neurosci* 12:389.
- Tominaga Y, Taketoshi M, Maeda N, Tominaga T (2019) Wide-field single-photon optical recording in brain slices using voltage-sensitive dye. *J Vis Exp* 148:e59692.
- Tominaga T, Kajiwara R, Tominaga Y (2023) Stable wide-field voltage imaging for observing neuronal plasticity at the neuronal network level. *Biophys Physicobiol* 20:e200015.
- Tovar-Moll F, Moll J, de Oliveira-Souza R, Bramati I, Andreiuolo PA, Lent R (2007) Neuroplasticity in human callosal dysgenesis: a diffusion tensor imaging study. *Cereb Cortex* 17:531–541.
- Yizhar O, Fenno LE, Davidson TJ, Mogri M, Deisseroth K (2011) Optogenetics in Neural Systems. *Neuron* 71:9–34.
- Utsumi Y, Taketoshi M, Miwa M, Tominaga Y, Tominaga T (2023) Assessing seizure liability *in vitro* with voltage-sensitive dye imaging in mouse hippocampal slices. *Front Cell Neurosci* 17:1217368.
- van Heukelum S, Mars RB, Guthrie M, Buitelaar JK, Beckmann CF, Tiesinga PHE, Vogt BA, Glennon JC, Havenith MN (2020) Where is cingulate cortex? A cross-species view. *Trends Neurosci* 43:285–299.
- Vogt BA, Pandya DN (1987) Cingulate cortex of the rhesus monkey: II. Cortical afferents. *J Comp Neurol* 262:271–289.
- Walker J, Storch G, Quach-Wong B, Sonnenfeld J, Aaron G (2012) Propagation of epileptiform events across the corpus callosum in a cingulate cortical slice preparation. *PLoS One* 7:e31415.
- Yan Z, Rein B (2022) Mechanisms of synaptic transmission dysregulation in the prefrontal cortex: pathophysiological implications. *Mol Psychiatry* 27:445–465.
- Yoshimura H, Sugai T, Kato N, Tominaga T, Tominaga Y, Hasegawa T, Yao C, Akamatsu T, (2016) Interplay between non-NMDA and NMDA receptor activation during oscillatory wave propagation: analyses of caffeine-induced oscillations in the visual cortex of rats. *Neural Netw* 79:141–149.
- Yuste R, (2008) Circuit neuroscience: the road ahead. *Front Neurosci* 2:6–9.